Sensitivity improvement of aluminum-based far-ultraviolet nearly guided-wave surface plasmon resonance sensor

Tianqi Li(李天琦)[1], Shujing Chen(陈淑静)[2,†], and Chengyou Lin(林承友)[1,‡]

[1] *College of Mathematics and Physics, Beijing University of Chemical Technology, Beijing* 100029, *China*
[2] *School of Materials Science and Technology, China University of Geosciences (Beijing), Beijing* 100083, *China*

(Received 25 December 2021; revised manuscript received 10 August 2022; accepted manuscript online 16 August 2022)

An aluminum (Al) based nearly guided-wave surface plasmon resonance (NGWSPR) sensor is investigated in the far-ultraviolet (FUV) region. By simultaneously optimizing the thickness of Al and dielectric films, the sensitivity of the optimized Al-based FUV-NGWSPR sensor increases from 183°/RIU to 309°/RIU, and its figure of merit rises from 26.47 RIU^{-1} to 32.59 RIU^{-1} when the refractive index of dielectric increases from 2 to 5. Compared with a traditional FUV-SPR sensor without dielectric, the optimized FUV-NGWSPR sensor can realize simultaneous improvement of sensitivity and figure of merit. In addition, the FUV-NGWSPR sensor with realistic materials (diamond, Ta_2O_5, and GaN) is also investigated, and 137.84%, 52.70%, and 41.89% sensitivity improvements are achieved respectively. This work proposes a method for performance improvement of FUV-SPR sensors by exciting nearly guided-wave, and could be helpful for the high-performance SPR sensor in the short-wavelength region.

Keywords: surface plasmon resonance sensor, far-ultraviolet, nearly guided-wave, sensitivity

PACS: 42.81.Pa, 78.20.–e, 07.60.–j, 95.85.Mt **DOI:** 10.1088/1674-1056/ac89e0

1. Introduction

Ultraviolet plasmonics exhibits a promising application,[1] in such as fluorescence,[2] photoelectron emission,[3] Raman scattering,[4] and biochemical sensing,[5] due to the higher energy and the more abundant molecular electronic transitions compared with visible plasmonics.[6] Surface plasmon resonance (SPR) sensors detect the change of refractive index near the surface of metal film as the change of reflected light intensity, which is caused by SPR wavelength or angle shift.[7] In present, SPR sensors have received extensive attention in the fields of biomedicine,[8] food safety,[9] and environmental detection[10] owing to unique features such as high sensitivity, no labeling, real time, and fast analysist speed.

Recently, deep-ultraviolet (DUV, 200 nm–300 nm) and far-ultraviolet (FUV, 120 nm–200 nm) SPR sensors have developed rapidly,[11,12] because some target molecules such as protein shows strong absorption and high refractive index only in the FUV-DUV region.[13] Strong absorption and high refractive index of target molecules could both improve the change of environment refractive index, which is beneficial for forming large angle or wavelength shift.[14] Also, the FUV-DUV-SPR sensors improve the surface measurement accuracy over that of the visible-SPR sensors, because the penetration depth of the evanescent wave is much short in the FUV-DUV region.[15] Therefore, the FUV-DUV-SPR sensor has significant characteristics, such as high sensitivity, material selectivity and surface specificity.[14]

The plasma frequency (2.4×10^{16} s^{-1})[16] of aluminum (Al) is higher than the light frequency in the FUV-DUV region making it a common-used metal for UV-SPR sensors. Gold and silver thin films are usually used for visible-SPR sensors because of their plasma frequency (1.37×10^{16} s^{-1} and 1.36×10^{16} s^{-1}).[17] Surface plasmons excited by light in the FUV region have already been investigated. Callcott and Arakawa measured photo yield of polarized light incident on thin Al film through an MgF semicylinder as a function of incident angle to study SPR in the wavelength range of 100 nm–300 nm.[18] Endriz and Spicer obtained the evidence of changes in SPR characteristics in the photoelectric emission measurements of slightly rough aluminum surface with light wavelengths from 120 nm to 200 nm.[19] Ichiro *et al.* studied the wavelength dependence on the refractive index of prisms (quartz and sapphire) and materials placed on Al thin films (air, HFIP, water, and sucrose water solutions) for an Al-based SPR sensor.[20] Moreira *et al.* replaced indium film to aluminium film, added gold layer and added graphene layer to realize the performance improvement of UV-SPR sensors through theoretical simulation.[21]

As one of the most important parameters of an SPR sensor, sensitivity is generally defined as the resonance angle or wavelength shift per sample refractive index unit (RIU). The work of improving sensitivity of the FUV-SPR sensor attracts increasing interests. Some ways have already been used for sensitivity improvement of an SPR sensor, like employing graphene-based multilayer structure,[22] phase-sensitive surface plasmon resonance,[23] and adding grating on top of the

†Corresponding author. E-mail: chenshujing@cugb.edu.cn
‡Corresponding author. E-mail: cylin@mail.buct.edu.cn

© 2022 Chinese Physical Society and IOP Publishing Ltd

metal layer.[24] Lahav *et al.*[25] excited nearly guided-wave SPR (NGWSPR) by using a Si film with high refractive index between the metal film and the sample, thereby achieving increased sensitivity. Shukla *et al.*[26] and Bao *et al.*[27] studied that the sensitivity of fiber-type and prism-type SPR sensors were significantly enhanced by adding the ZnO layer on top of the metal layer respectively. Benkebou *et al.*[28] adopted the multilayer structure of dielectric in the SPR sensor to improve sensitivity.

In this paper, sensitivity improvement of Al-based NGWSPR sensors with different dielectric is studied in the FUV region. To improve the sensitivity of the proposed FUV-NGWSPR sensor, the thickness of the Al and dielectric film are simultaneously optimized. Then, the optimized performance parameters of the proposed sensor are investigated and compared for the NGWSPR sensors with different dielectric refractive index. Furthermore, the performance of Al-based FUV-NGWSPR sensors with diamond, Ta_2O_5 and GaN are studied comparatively and the origin of sensitivity improvement is determined. The method to improve performance of SPR sensors in the ultraviolet region by exciting nearly guided-wave is significant for the design of high-performance UV-SPR sensors.

2. Theory

2.1. FUV-NGWSPR sensor

The proposed FUV-NGWSPR sensor (see Fig. 1) uses Kretschmann configuration[29] to excite NGWSPR and is based on angular interrogation.

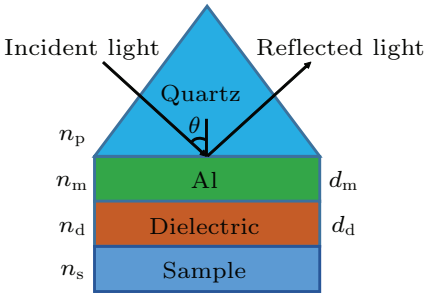


Fig. 1. The schematic diagram of the proposed Al-based FUV-NGWSPR sensor.

A monochromatic FUV light from deuterium lamp of wavelength 185 nm is considered to be the source.[14] In this sensor, the quartz glass prism is sequentially coated with metal and dielectric, so there are two layers on the prism. Al is considered to be the active metal in the sensor. In order to excite the NGWSPR in the sensor, different materials as the dielectric film are considered. The sensing medium, which is assumed to be water with ss-DNA biomolecules for our simulations, keeps in contact with the dielectric film. The dielectric film can adsorb the biomolecules on its surface to cause the surface refractive index to increase locally ($\Delta n = 0.005$). The refractive index and extinction coefficient of all materials used in the proposed NGWSPR sensor are list in Table 1.

Table 1. Refractive index and extinction coefficient of used materials at 185 nm.

Material	Refractive index (n)	Extinction coefficient (k)	Ref.
Quartz	1.5832	0	[14]
Al	0.1075	2.0359	[14]
Diamond	3.0513	0.025176	[30]
Ta_2O_5	1.9149	0.8887	[31]
GaN	2.8111	1.6935	[32]
Water	1.4576	0	[33]

2.2. Reflectivity

For reflectivity calculation, the proposed FUV-NGWSPR sensor composed of prism, metal, dielectric and sample can be regarded as a 4-layer structure, so the transfer matrix method is used to get the formula of reflectivity. The tangential components of electric and magnetic field amplitudes at the quartz–Al interface (E_1 and H_1) are connected to those at the dielectric-sample interface (E_3 and H_3) by the matrix

$$\begin{bmatrix} E_1 \\ H_1 \end{bmatrix} = \begin{bmatrix} \cos\delta_m & \frac{\mathrm{i}}{\eta_m}\sin\delta_m \\ \mathrm{i}\eta_m \sin\delta_m & \cos\delta_m \end{bmatrix} \times \begin{bmatrix} \cos\delta_d & \frac{\mathrm{i}}{\eta_d}\sin\delta_d \\ \mathrm{i}\eta_d \sin\delta_d & \cos\delta_d \end{bmatrix} \begin{bmatrix} E_3 \\ H_3 \end{bmatrix}, \quad (1)$$

where δ_m (or δ_d) and η_m (or η_d) are the phase factor and the optical admittance of the metal (or dielectric) film. $\delta_a = 2\pi n_a d_a \cos\theta_a/\lambda$ ($a =$ m or d) is the phase factor, in which n_a and d_a ($a =$ p, m, d, s) represent the refractive index and thickness of each layer in the 4-layer structure. λ represents the wavelength of incident light and θ_a represents the angle of incident light in each layer. $\eta_a = n_a/\cos\theta_a$ ($a =$ p, m, d, s) is the optical admittance for p-polarized light.

Because $H_3/E_3 = \eta_s$ and $H_1/E_1 = Y$ (the equivalent optical admittance of the assembly), equation (1) can also be expressed as

$$E_1 \begin{bmatrix} 1 \\ Y \end{bmatrix} = \begin{bmatrix} \cos\delta_m & \frac{\mathrm{i}}{\eta_m}\sin\delta_m \\ \mathrm{i}\eta_m \sin\delta_m & \cos\delta_m \end{bmatrix} \times \begin{bmatrix} \cos\delta_d & \frac{\mathrm{i}}{\eta_d}\sin\delta_d \\ \mathrm{i}\eta_d \sin\delta_d & \cos\delta_d \end{bmatrix} \begin{bmatrix} 1 \\ \eta_s \end{bmatrix} E_3. \quad (2)$$

The characteristic matrix of the structure can be written as

$$\begin{bmatrix} B \\ C \end{bmatrix} = \begin{bmatrix} \cos\delta_m & \frac{\mathrm{i}}{\eta_m}\sin\delta_m \\ \mathrm{i}\eta_m \sin\delta_m & \cos\delta_m \end{bmatrix} \times \begin{bmatrix} \cos\delta_d & \frac{\mathrm{i}}{\eta_d}\sin\delta_d \\ \mathrm{i}\eta_d \sin\delta_d & \cos\delta_d \end{bmatrix} \begin{bmatrix} 1 \\ \eta_s \end{bmatrix}. \quad (3)$$

The reflectivity R of this structure can be calculated as

$$R = \left| \frac{\eta_p B - C}{\eta_p B + C} \right|^2. \tag{4}$$

The curve of reflectivity R with incident angle can be got.

2.3. Performance parameters

The incident angle is called the resonance angle θ_{res} when the minimum reflectance (R_{res}) is realized. The angular sensitivity (S) of the sensor is expressed as the ratio between the resonance angle variation ($\Delta\theta_{res}$) and the refractive index variation of the sample (Δn_s),

$$S = \frac{\Delta\theta_{res}}{\Delta n_s}. \tag{5}$$

The linewidth is generally expressed by the full width at half maximum (FWHM) of the resonant peak, that is, the distance between two angle points corresponding to the normalized light intensity half-height. Narrower FWHM can lead to a higher detection accuracy,

$$\text{FWHM} = \Delta\theta_{0.5}. \tag{6}$$

The figure of merit (FOM) is a comprehensive parameter to measure the performance of the sensor, which is defined as the ratio of sensitivity to FWHM,

$$\text{FOM} = \frac{S}{\text{FWHM}}. \tag{7}$$

3. Results and discussion

3.1. Optimized thickness for sensitivity improvement

To improve sensitivity of the Al-based FUV-NGWSPR sensor, a dielectric film with the refractive index of 2.5 is added on top of Al film as a start. The sensitivity of the proposed FUV-NGWSPR sensor is investigated by simultaneously changing the thickness of Al (d_m) and dielectric film (d_d), as shown in Fig. 2. It is seen that with the change of metal and dielectric film thickness, the sensitivity of FUV-NGWSPR sensor exhibits a series of optimized sensitivity values, locating at the crest of curve.

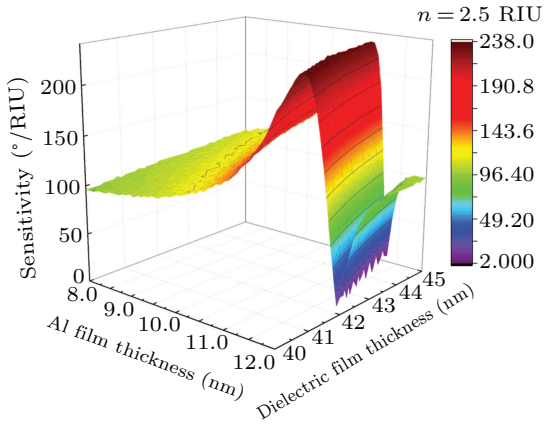


Fig. 2. Sensitivity as a function of Al and dielectric ($n = 2.5$) film thickness for the Al-based NGWSPR sensor.

To further investigate the sensitivity enhancement by optimizing thickness of metal and dielectric film, the optimized sensitivities and their corresponding d_d and d_m in Fig. 2 are shown in Fig. 3. When d_m increases from 4 nm to 35 nm, d_d always decreases from 49.2 nm to 40.3 nm, indicating that there is a trade-off between d_m and d_d for sensitivity optimization. However, the optimized sensitivity increases at first and then decreases, showing its maximum value ($S_{max} = 238°$/RIU) when $d_m = 9.9$ nm and $d_d = 44.3$ nm. In this case, FWHM and FOM of this sensor are also investigated, and which are 8.8803° and 26.80 RIU^{-1} respectively.

As seen that the optimized sensitivity of the proposed SPR sensor increases from 146°/RIU to 238°/RIU as d_m increases from 4 nm to 9.9 nm at first and then decreases from 238°/RIU to 141°/RIU as d_m increases from 9.9 nm to 35 nm, but d_d always decreases from 49.2 nm to 40.3 nm. It seems that there is a trade-off between d_m and d_d. One film thickness (such as Al film) in the two layers increases, the other film thickness (such as dielectric film) reduces accordingly to enable the proposed SPR sensor to obtain high sensitivity. Therefore, the total thickness of the two layers is limited for achieving optimized sensitivity.

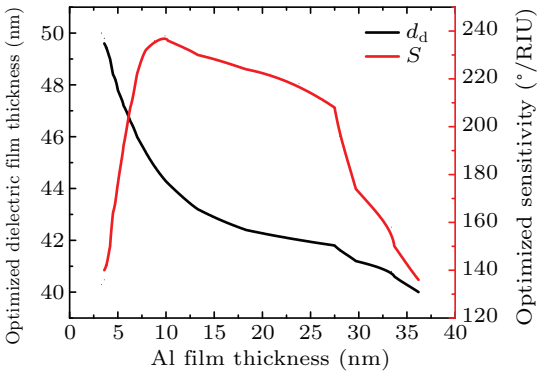


Fig. 3. Optimized sensitivity and its corresponding Al and dielectric film thickness.

3.2. Optimized dielectric for sensitivity improvement

Using the same method as above, S_{max} of the Al-based NGWSPR sensor with different dielectric refractive indexes can be found. When S_{max} is achieved, optimal thickness of Al (d_m) and dielectric film (d_d) for the refractive index (n) of the dielectric varied from 2 to 5 in an interval of 0.5 are shown in Fig. 4. When n increases from 2 to 5, d_m fluctuates around 10 nm, but d_d decreases from 70 nm to 18.3 nm.

In Fig. 5, optimized parameters of the proposed FUV-NGWSPR sensor achieving maximum sensitivity for different refractive indexes of the dielectric film are shown. For comparisons, the performance parameters of a traditional Al-based SPR sensor with optimized thickness of Al film, which does

not use a dielectric film to excite NGWSPR, is also exhibited in Fig. 5. Its maximum sensitivity S_{max} (74°/RIU) shows when $d_m = 5.6$ nm, and its corresponding FWHM and FOM are 7.5346° and 9.8214 RIU^{-1} respectively.

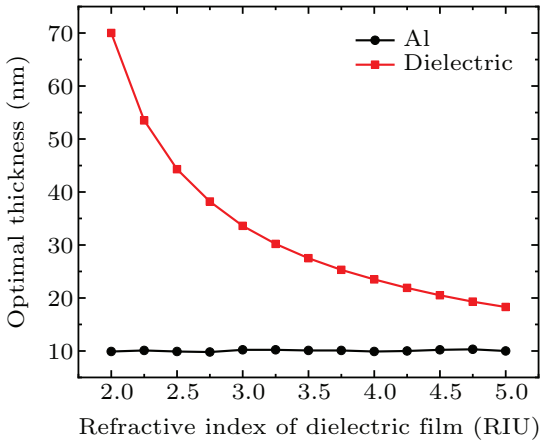


Fig. 4. Optimal Al and dielectric film thicknesses for dielectric film of different refractive index.

In Fig. 5(a), S_{max} shows an upward trend with the increase of n. When n increases from 2 to 5, S_{max} increases from 183°/RIU to 309°/RIU, and is always greater than the one of the traditional FUV-SPR sensor (74°/RIU). In Fig. 5(b), FWHM corresponding S_{max} increases rapidly with n at first, then fluctuates around 9.5°. Although FWHM of NGWSPR sensor is not narrower than the one of SPR senor except the case of $n = 2.0$, FOM of NGWSPR sensor is always higher, as shown in Fig. 5(c). In addition, when n increases from 2 to 5, FOM increases from 26.47°/RIU to 32.59°/RIU. This result is interesting because the simultaneous improvement of sensitivity and FOM can be achieved by a NGWSPR sensor operated in the FUV region, which has not been found in other spectral region such as visible and infrared bands.[7,34] Compared with a traditional SPR sensor, the improvement of sensitivity is attributed to the excitation of nearly-guided waves in the NGWSPR sensor, while the enhancement of FOM originates from the higher increment of sensitivity than the one of FWHM in the FUV region when a dielectric film with high refractive index is added in the Al-based sensor.

Generally, the increase of the sensitivity of the sensor, but also broaden the resonance dip and leads to the increase of FWHM. However, in this Al-based FUV NGWSPR sensor, the increase of sensitivity is higher than the increase of FWHM of low refractive index and high extinction coefficient of Al, and the use of nearly guided-wave surface plasmon resonance.

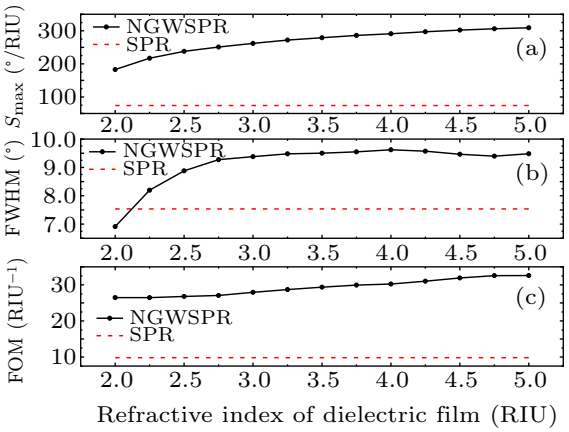


Fig. 5. (a) Sensitivity, (b) FWHM and (c) FOM of optimized Al-based NGWSPR sensor for different dielectric refractive index.

3.3. FUV-NGWSPR sensor with different dielectric materials

Basing on the results above, three realistic materials (diamond, Ta_2O_5, and GaN) are selected as the dielectric for an Al-based FUV-NGWSPR sensor. Similar parameters optimization is performed for each material, and optimized performance parameters of optimized NGWSPR sensors are listed in Table 2. It is seen that FUV-NGWSPR sensors with three materials all realize sensitivity improvement compared with the one of the traditional FUV-SPR sensor without dielectric. Sensitivities increase by 137.84%, 52.70%, and 41.89% respectively for diamond, Ta_2O_5 and GaN compared to that without dielectric. The FUV-NGWSPR sensor with diamond achieve the highest sensitivity (176°/RIU) and FOM (16.12 RIU^{-1}), which are both higher than that without the dielectric. The sensitivity is 29°/RIU and 15°/RIU higher than that of two different reported UV-SPR sensors.[35] In addition, the angular spectrums, which is the reflectivity curves as a function of incident angle, of the optimized FUV-NGWSPR sensors with diamond, Ta_2O_5, GaN and the optimized FUV-SPR sensor without dielectric are also plotted, as shown in Fig. 6. Four curves all exhibit large depth of dip ($R_{res} < 10\%$), indicating good signal-to-noise ratio (SNR) for sensing.[36] The resonance angle of the high-sensitivity FUV-NGWSPR sensor with diamond is the smallest, and it is the largest for the traditional FUV-SPR sensor without dielectric.

Table 2. Performance parameters of optimized Al-based NGWSPR sensors.

Dielectric	d_m (nm)	d_d (nm)	θ_{res} (°)	R_{res}	S (°/RIU)	FWHM (°)	FOM (RIU^{-1})
Without	5.6	0	88.19	0.0788	74	7.53	9.82
Diamond	11.4	32.2	80.78	0.0308	176	10.91	16.12
Ta_2O_5	4.4	1.1	84.99	0.0923	113	14.33	7.88
GaN	3.7	1.3	84.13	0.0958	105	14.58	7.20

In addition, the effect of interfacial roughness (i-r) on the reflectivity of optimized Al-based NGWSPR sensors is study by multiplying the reflectivity by Debye–Waller factor,[37] as shown in Fig. 6. It is seen that the interface roughness has little effect on each reflectivity curve, demonstrating that good stability of performance of optimized sensors for interfacial roughness.

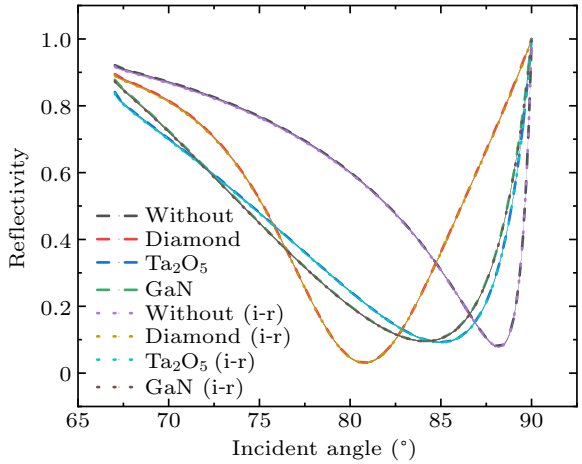


Fig. 6. Reflectivity curves as a function of incident angle of optimized FUV-NGWSPR sensors with diamond, Ta_2O_5, GaN, and optimized FUV-SPR sensor without dielectric.

To investigate the origin of sensitivity improvement, the tangential electric field intensity of the optimized FUV-NGWSPR sensors for three dielectric materials are calculated using the method described by Shalabney and Abdulhalim,[38] as shown in Fig. 7. It is seen that the case which exhibits a larger value of the tangential electric field intensity at the dielectric-sample interface always shows a higher sensitivity by comparing the sensitivity and the tangential electric field intensity of the sensors for different dielectric materials. The results indicate that sensitivity improvement of the optimized sensors is attributed to the tangential electric field intensity enhancement.

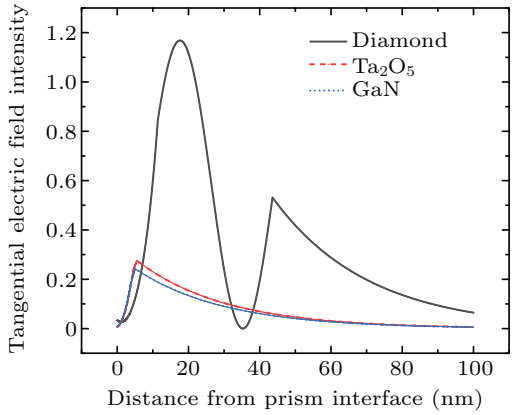


Fig. 7. Tangential electric field intensity of optimized FUV-NGWSPR sensors with diamond, Ta_2O_5, and GaN.

4. Conclusion

In summary, the Al-based FUV-NGWSPR sensor with optimized Al and dielectric film for performance improvement has been theoretically investigated in this paper. Above all, by simultaneously optimizing the thickness of Al and dielectric film, the maximum sensitivity of the proposed SPR sensor with dielectric film of the refractive index of 2.5 has been found. When the thickness of Al film increases from 4 nm to 35 nm, the optimized sensitivity increases from 146°/RIU to 238°/RIU firstly and then decreases to 141°/RIU, but the thickness of dielectric film decreases from 49.2 nm to 40.3 nm. The results indicate that there is a trade-off between thickness of Al and dielectric films for maximum sensitivity. Then, the Al-based FUV-NGWSPR sensor with different dielectric refractive index is optimized for maximum sensitivity. It is worth noting that the sensitivity and FOM of optimized FUV-NGWSPR sensor both increase with the increase of dielectric refractive index, reaching maximum values of 309°/RIU and 32.59 RIU^{-1} respectively. At last, Al-based FUV-NGWSPR sensors with three realistic materials (diamond, Ta_2O_5, and GaN) are investigated. All sensors realize sensitivity improvement. The FUV-NGWSPR sensor with diamond achieves the highest sensitivity (176°/RIU) and FOM (16.12 RIU^{-1}), which are both higher than that without the dielectric. Compared with previously published UV-SPR sensor schemes, the optimized sensor with diamond provides a higher sensitivity. Also, all reflectivity curves of FUV-NGWSPR sensors exhibit large depth of dip, indicating good signal-to-noise ratio for sensing. By comparing the sensitivity and the electric field intensity of the optimized sensors with different dielectric materials, it is demonstrated that sensitivity improvement of the optimized sensor is attributed to the electric field intensity enhancement. This paper provides a way for designing highly-sensitive UV-SPR sensors by exciting nearly guided-wave and is of significance for the development of high-performance SPR sensors.

Acknowledgement

Project supported by the National Natural Science Foundation of China (Grant Nos. 61805007 and 11547241).

References

[1] Martin J, Proust J, Gerard D and Plain J 2013 *Opt. Mater. Express* **3** 954
[2] Lakowicz J R, Shen B, Gryczynski Z, D'Auria S and Gryczynski I 2001 *Biochem. Biophys. Res. Commun.* **286** 875
[3] Watanabe Y, Inami W and Kawata Y 2011 *J. Appl. Phys.* **109** 023112
[4] Jha S K, Ahmed Z, Agio M, Ekinci Y and Löffler J F 2012 *J. Am. Chem. Soc.* **134** 1966
[5] Norek M, Wlodarski M and Matysik P 2014 *Curr. Appl. Phys.* **14** 1514
[6] Tanabe I, Shimizu M, Kawabata R, Katayama C and Fukui K 2019 *Sens. Actuators A* **301** 111661
[7] Meng Q Q, Zhao X, Chen S J, Lin C Y, Ding Y C and Chen Z Y 2017 *Chin. Phys. B* **26** 124213
[8] Beland P and Berini P 2017 *Appl. Phys. A-Mater.* **123** 31
[9] Piliarik M, Párová L and Homola J 2009 *Biosens. Bioelectron.* **24** 1399
[10] Farré M, Kantiani L and Barceló D 2007 *Trends Anal. Chem.* **26** 1100
[11] Knight M W, King N S, Liu L F, Everitt H O, Nordlander P and Halas N J 2014 *ACS Nano* **8** 834

[12] Kumamoto Y, Taguchi A, Honda M, Watanabe K, Saito Y and Kawata S 2014 *ACS Photon.* **1** 598
[13] Goto T, Ikehata A, Morisawa Y and Ozaki Y 2013 *J. Phys. Chem. A* **117** 2517
[14] Tanabe I, Tanaka Y Y, Ryoki T, Watari K, Goto T, Kikawada M, Inami W, Kawata Y and Ozaki Y 2016 *Opt. Express* **24** 21886
[15] Tanabe I, Tanaka Y Y, Watari K, Hanulia T, Goto T, Inami W, Kawata Y and Ozaki Y 2017 *Chem. Lett.* **46** 1560
[16] Rakić A D 1995 *Appl. Opt.* **34** 4755
[17] Johnson P B and Christy R W 1972 *Phys. Rev. B* **6** 4370
[18] Callcott T A and Arakawa E T 1975 *Phys. Rev. B* **11** 2750
[19] Endriz J G and Spicer W E 1970 *Phys. Rev. Lett.* **24** 64
[20] Tanabe I, Tanaka Y Y, Watari K, Hanulia T, Goto T, Inami W, Kawata Y and Ozaki Y 2017 *Sci. Rep.* **7** 5934
[21] Moreira C, Wang Y S, Blair S, Chadwick E, Lee J Y, Oliveira L, Lima A and Cruz R S 2020 *Opt. Lett.* **45** 4642
[22] Maharana P K, Jha R and Palei S 2014 *Sens. Actuators B* **190** 494
[23] Lin C Y and Chen S J 2019 *Opt. Commun.* **445** 155
[24] Alleyne C J, Kirk A G, McPhedran R C, Nicorovici N A P and Maystre D 2007 *Opt. Express* **15** 8163
[25] Lahav A, Auslender M and Abdulhalim I 2008 *Opt. Lett.* **33** 2539
[26] Shukla S, Sharma N K and Sajal V 2015 *Sens. Actuators B* **206** 463
[27] Bao M, Li G, Jiang D, Cheng W and Ma X 2012 *Appl. Phys. A* **107** 279
[28] Benkabou F and Chikhi M 2014 *Phys. Status Solidi A* **211** 700
[29] Gwon H R and Lee S H 2010 *Mater. Trans.* **51** 1150
[30] Phillip H R and Taft E A 1964 *Phys. Rev.* **136** A1445
[31] Marcos R D, Larruquert J I, Méndez J A and Aznárez J A 2016 *Opt. Mater. Express* **6** 3622
[32] Pastrňák J and Roskovcová L 1966 *Phys. Status Solidi* **14** K5
[33] Daimon M and Masumura A 2007 *Appl. Opt.* **46** 3811
[34] Chen S J and Lin C Y 2019 *Opt. Commun.* **435** 102
[35] Moreira C, Wang Y S, Blair S, Carvalho I and Cruz R S 2020 *Plasmonics* **15** 1891
[36] Shalabney A and Abdulhalim I 2011 *Laser Photon. Rev.* **5** 571
[37] Vidal B and Vincent P 1984 *Appl. Opt.* **23** 1794
[38] Shalabney A and Abdulhalim I 2010 *Sens. Actuators A* **159** 24